Supporting Information for

Critical Aspects of Heme-Peroxo-Cu Complex Structure and Nature of Proton Source Dictate Metal–O_{peroxo} Breakage vs. Reductive O–O Cleavage Chemistry

Suzanne M. Adam,[†] Isaac Garcia-Bosch,[†] Andrew W. Schaefer,[‡] Savita K. Sharma,[†] Maxime A. Siegler, Edward I. Solomon,[*,‡] and Kenneth D. Karlin[*,†]

Table of Contents:

1. H_2O_2 quantification by Horseradish Peroxidase (HRP) test. The reaction mixtures were subjected to H_2O_2 analysis as described in the Experimental Section. Results of the quantification are shown in **Table S1**.

Table S1. H_2O_2 quantification for the iron-peroxo-copper species at different conditions.

LS complex (0.1mM)	[4-NO_2-phenol] (mM)	[Fc*] (mM)	H_2O_2 (%)
(**LS-4DCHIm**)	-	-	95
(**LS-4DCHIm**)	2	-	85
(**LS-4DCHIm**)	2	2	0
(**LS-3DCHIm**)	-	-	100
(**LS-3DCHIm**)	2	2	90

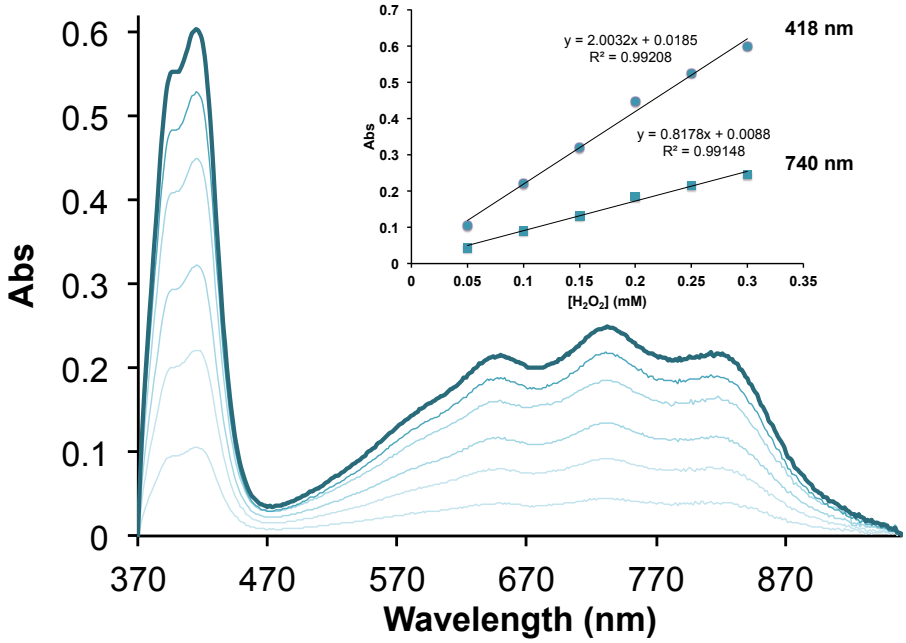

Figure S1. Calibration curve used for H_2O_2 quantification by the HRP method.[1]

2. Strong acid ([DMF·H$^+$](CF$_3$SO$_3^-$)) (p*K*a (CH$_3$CN) = 0.7) reactivity. The reactions of **LS-4DCHIm** (-90°C) and **LS-3DCHIm** (-125°C) with strong acid were monitored by UV-Vis, EPR and rR spectroscopies in MeTHF. In both cases, addition of two equiv acid immediately releases H_2O_2 (**Table S1**), leaving $(DCHIm)_2F_8Fe(III)$ (λ_{max} = 542 nm) and $Cu(II)(DCHIm)_n(L)$ (λ_{max} = 900 nm (broad)) where L = DCHIm or MeTHF (**Figure S2**). Formation of the described products was confirmed by comparison of the reaction product spectra (UV-vis and EPR) to spectra of control samples containing a mixture of independently isolated $Cu^{II}(DCHIm)_4(ClO_4)_2$ and $F_8Fe^{III}{\cdot}SbF_6$ [2] in the presence of 1 excess equiv DCHIm. See pages **S7-8** for synthesis and characterization of $Cu^{II}(DCHIm)_4{\cdot}(ClO_4)_2$.

The rR spectra of the reaction products of **LS-3DCHIm** or **LS-4DCHIm** plus [DMF·H$^+$](CF$_3$SO$_3^-$) showed no isotope sensitive vibrations (metal-associated $^{16}O_2$ vs. $^{18}O_2$ species).

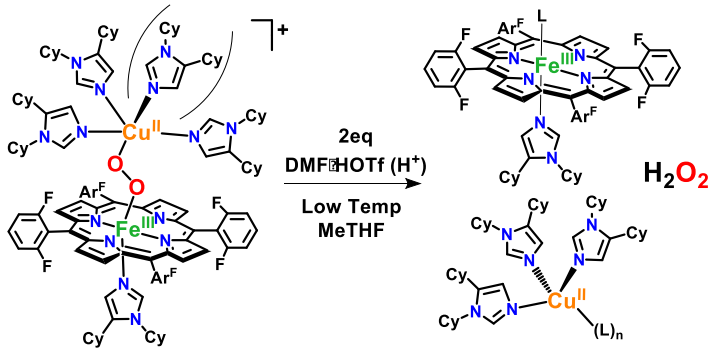

Figure S2. Proposed reaction and products when LS heme-peroxo-copper complexes are reacted with [DMF·H$^+$](CF$_3$SO$_3^-$).[3]

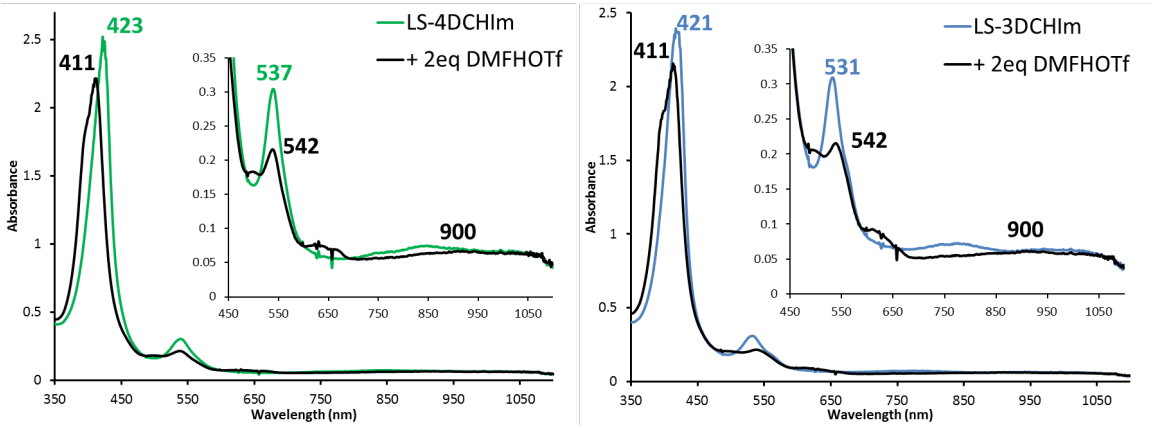

Figure S3. UV-vis spectra showing the initial and final spectra from a reaction of **LS-4DCHIm** (left) and **LS-3DCHIm** (right) with 2 eq. [DMF·H$^+$](CF$_3$SO$_3^-$) to form the reaction products in **Figure S3** (**black** spectra). The **black** product spectra match with that of an authentic mixture of independently isolated $Cu^{II}(DCHIm)_4{\cdot}(ClO_4)_2$ (900 nm, broad) and $F_8Fe^{III}{\cdot}SbF_6$ in the presence of 1 or 2 excess equiv DCHIm (542 nm). See page **S7**.

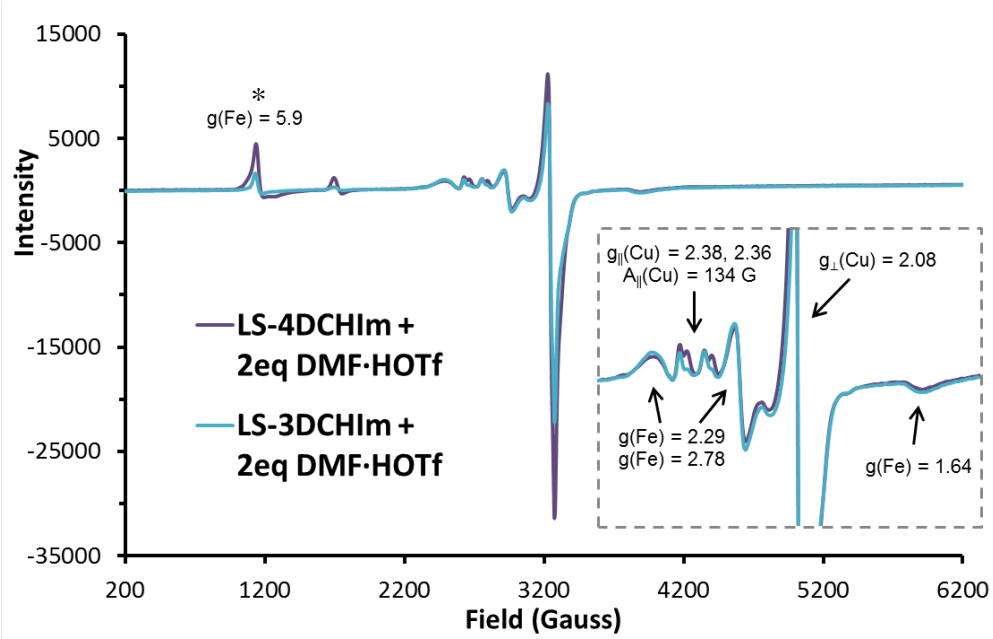

Figure S4. EPR spectra of the reaction products of **LS-3DCHIm** (**purple**) and **LS-4DCHIm** (**blue**) with strong acid, [DMF·H^+]($CF_3SO_3^-$), showing identical products, those being species depicted in **Figure S2**.

These spectra are representative of 90-100% yield of $Cu^{II}(DCHIm)_n$-L (g = 2.08, 2.36, 2.38) (L = MeTHF, or DCHIm), and 60-65% low-spin $Fe^{III}(DCHIm)_2$ (g = 2.29, 2.78, 1.64) with a small amount (~5-15%) of high-spin Fe(III) (g = 5.9). These yield ranges encompass the quantification for these species in the reactions of both **LS-3DCHIm** and **LS-4DCHIm** with [DMF·H^+]($CF_3SO_3^-$), and were calculated via spectral addition (as outlined on **p.S12**) based on the observation that intensities and g-values of these EPR signals match closely with authentic samples at the same concentration used for experiments (2 mM for authentic mononuclear heme and copper complexes (**Figure S11**), and for the **LS-3DCHIm**, **LS-4DCHIm** complexes). (See pages **S7-8** for details regarding generation of the authentic product mixture). We propose the relatively low yield of Fe(III) signal may be due to rebinding of the H_2O_2 released in the reaction to the Fe to form a stable Fe(III)-(O_2^{2-})-Fe(III) species which would be EPR silent.
*If a full equiv of HS-heme complex (g = 5.9) formed, the intensity of that signal in these experimental spectra would be ~15x greater.

3. Resonance Raman $^{16}O_2$–$^{18}O_2$ difference spectra of **LS-4DCHIm (black)** and the phenol-associated adduct, **[LS-4DCHIm(ArOH)] (blue)** at high and low energy excitation. In both cases, *v*(Fe-O) and *v*(O-O) stretches are observed. Prepared at 1mM, at -90°C in MeTHF.

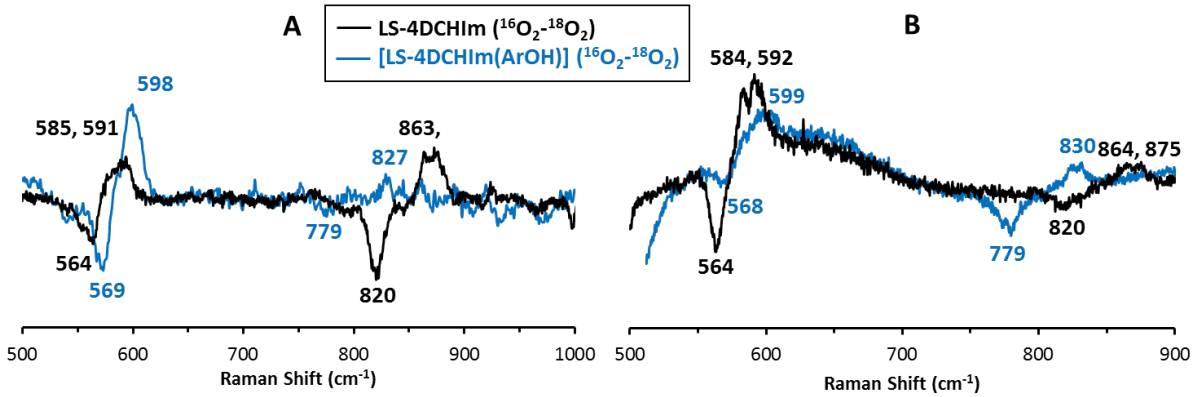

Figure S5. (A) Resonance Raman spectra of the **LS-4DCHIm** (**black**) and **[LS-4DCHIm(ArOH)]** (**blue**) at high energy excitation (413 nm for both). High energy excitation into the porphyrin Soret increases enhancement of the Fe-O stretch, (although remarkably the O-O stretch is still observable in both cases). **(B)** Low energy excitation into the CT band (870 nm for **LS-4DCHIm** and 815 nm for **[LS-4DCHIm(ArOH)]**) shows greater O-O enhancement. The H-bonding interaction lowers the energy of the peroxo orbitals, therefore, slightly lower excitation results in the optimum resonance enhancement for **[LS-4DCHIm(ArOH)].**

The low energy excitation spectrum for **[LS-4DCHIm(ArOH)]**, is also shown in the main text (**Figure 3**, bottom left), below the high energy excitation spectrum of **LS-4DCHIm** for optimum clarity of both species.

We also note that an Fe(III)-OH species impurity may contribute to increased intensity of the 598 cm^{-1} stretch (i.e. in **Figure S5(A)**).”

4. Authentic final products generation (UV-Vis, EPR): The iron and copper-containing final reaction products for both the strong and weak acid reactions with **LS-4DCHIm** and **LS-3DCHIm** were compared to authentically generated mixtures of the proposed products (**Figure 5** in text, **Figures S2, S6, S13**). That authentic mixture of these products can be prepared one of two ways, in situ (**A**, below) or from isolated metal-ligand complexes (**B**, next page)) yielding the same results.

A. In-situ generation of (DCHIm)F_8Fe^{III}-L + $Cu^{II}(DCHIm)_x$(L) (L = DCHIm, MeTHF)

After generation of **HS-3MeTHF** in a typical UV-Vis or EPR experiment at -90 ºC (analysis here shown by UV-vis), the solution was warmed under Ar, causing the decay of the peroxo complex to the high-spin iron(III)-aquo complex (**Figure S6**). After cooling, addition of different concentrations of DCHIm caused the formation of a band at 542 nm, assigned as a low-spin (DCHIm)F_8Fe^{III}(L) complex, the same reaction product observed in the H^+/e^- reactivity of the (**LS-4DCHIm**) complex (see main text). In order to fully form the (DCHIm)F_8Fe^{III}(L) complex, 6 equiv. of DCHIm were required, which suggested that part of the imidazole was coordinating to the "naked" copper(II) present in solution. Analysis of the low-energy bands (800-1100 nm) suggested the formation of a copper(II)-imidazolyl complex. Addition of Fc* and 4-NO_2-phenol to the mixture didn't lead to any observable spectral change.

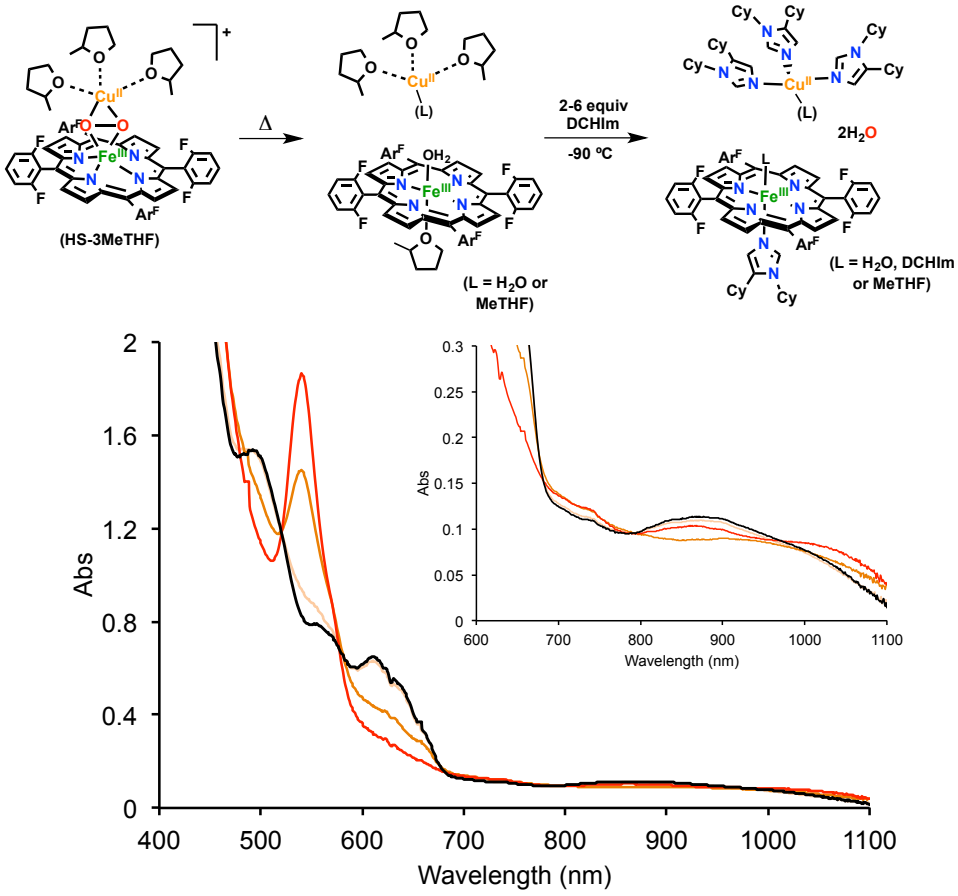

Figure S6. UV-Vis spectrum of the decay product of the high-spin peroxo complex (**HS-3MeTHF**) [0.135 mM] corresponding to the (MeTHF)$F_8Fe^{III}(H_2O)$ (**black spectra**). After cooling down (-90 ºC), sequential addition of 2 equiv. (**orange spectrum**), 4 equiv. (**orange spectrum**) and 6 equiv. of DCHIm (**red spectrum**) led to the formation of the complex $(DCHIm)_2F_8Fe^{III}$ (λ_{max} = 542 nm) along with the copper(II)-imidazolyl complex (800-1100 nm).

B. Generation of authentic mixture of products from isolated metal-ligand complexes: (A 1:1:1 mixture of $[(DCHIm)_4Cu^{II}]^{2+}$, $F_8Fe(III)SbF_6$ species,[2] and DCHIm)

In a typical UV-Vis or EPR experiment under Ar atmosphere at room temperature: To a solution of $F_8Fe(III)SbF_6$ was added 1 equiv $[(DCHIm)_4Cu^{II}](ClO_4)_2$ (see below for synthesis and crystallographic characterization) and one additional equivalent of DCHIm (to fit the stoichiometry of the reaction discussed in the text). EPR and UV-vis spectra showed a mixture of high-spin (F_8Fe^{III}(DCHIm)(MeTHF) or $F_8Fe^{III}(MeTHF)_2$) and low spin ($F_8Fe^{III}(DCHIm)_2$) ferric heme and Cu(II) signals (matching those for the independent components), and this authentic mixture matches well with those for the product mixtures of the heme-peroxo-copper complex reactions described in the text (**Figure 5** in text and see **Figure S11** for mononuclear species EPR spectra. The UV-vis spectrum of this mixture is identical to that of the in situ generation of these products shown in **Figure S6**, **red** spectrum).

Synthesis and characterization of $[(DCHIm)_4Cu^{II}](ClO_4)_2$: 0.5 ml of an acetone solution containing 87 mg of $Cu(II)(ClO_4)_2(H_2O)_6$ (0.22 mmols) were added dropwise to 0.5 mL of a solution where 200 mg of DCHIm had been dissolved (0.86 mmols). An immediate color change was observed (blue solution). The crude solution was stirred for 30 minutes, observing the formation of big pink crystals corresponding to the desired product. After several days, the acetone solution was separated and the crystalline product was dried under vacuum, obtaining 240 mg of product (Yield = 94%). Layering diethyl ether precipitated the acetone crude solution. A new batch of pink crystals was obtained, which were used for the X-ray diffraction analysis (see **Figure S7**).

- Elemental analysis: ($C_{60}H_{96}Cl_2CuN_8O_8$) Calculated: C, 60.5%; H, 8.1%; N, 9.4%. Found: C, 60.7%; H, 8.4%; N, 9.5%.
- ESI-MS: 527.32 $[(DCHIm)_2Cu^{I}]^+$ (also separately generated and characterized by X-ray crystallography (see below, **Figure S8**); 860.10 $[(DCHIm)_3Cu^{II}(ClO_4)]^+$; 1090.10 $[(DCHIm)_4Cu^{II}(ClO_4)]^+$.
- EPR: see **Figure S11**, g = 2.06, 2.34 (A = 164 G).

X-Ray characterization of $[(DCHIm)_4Cu^{II}](ClO_4)_2$

All reflection intensities were measured at 110(2) K using a SuperNova diffractometer (equipped with Atlas detector) with Cu *K*α radiation (λ = 1.54178 Å) under the program CrysAlisPro (Version 1.171.36.32 Agilent Technologies, 2013). The program CrysAlisPro (Version 1.171.36.32 Agilent Technologies, 2013) was used to refine the cell dimensions. Data reduction was done using the program CrysAlisPro (Version 1.171.36.32 Agilent Technologies, 2013). The structure was solved with the program SHELXS-2013 (Sheldrick, 2013) and was refined on F^2 with SHELXL-2013 (Sheldrick, 2013). Analytical numeric absorption corrections based on a multifaceted crystal model were applied using CrysAlisPro (Version 1.171.36.32 Agilent Technologies, 2013). The temperature of the data collection was controlled using the system Cryojet (manufactured by Oxford Instruments). The H atoms were placed at calculated positions using the instructions AFIX 13, AFIX 23, AFIX 43 or AFIX 137 with isotropic displacement parameters having values 1.2 or 1.5 times *U*eq of the attached C atoms.

The structure is mostly ordered. The Cu complex is located at sites of inversion symmetry, and only one half of the complex is crystallographically independent. One imidazole ring is disordered over two orientations (the second N atom of the imidazole ring can be found either on the third or fourth position, and the orientations "NC**N**CC" and "NCC**N**C" overlap). The occupancy factor of the major component of the disorder refines to 0.625(18). The lattice (uncoordinated) diethylether solvent molecule is found disordered over two orientations. The occupancy factor of the major component of the disorder refines to 0.811(6).

xs0177a: Fw = 1340.12, purple block, 0.32 × 0.27 × 0.24 mm^3, monoclinic, $P2_1/c$ (no. 14), a = 10.79777(8), b = 18.02876(11), c = 18.36383(14) Å, β = 95.7982(7)°, V = 3556.60(4) $Å^3$, Z = 2, D_x = 1.251 g cm^{-3}, μ = 1.606 mm^{-1}, abs. corr. range: 0.669–0.753. 28519 Reflections were measured up to a resolution of $(\sin \theta/\lambda)_{max}$ = 0.62 $Å^{-1}$. 6965 Reflections were unique (R_{int} = 0.0190), of which 6642 were observed [$I > 2\sigma(I)$]. 448 Parameters were refined using 139 parameters. $R1/wR2$ [$I > 2\sigma(I)$]: 0.0402/0.1115. $R1/wR2$ [all refl.]: 0.0415/ 0.1126. S = 1.036. Residual electron density found between −0.59 and 0.71 e $Å^{-3}$.

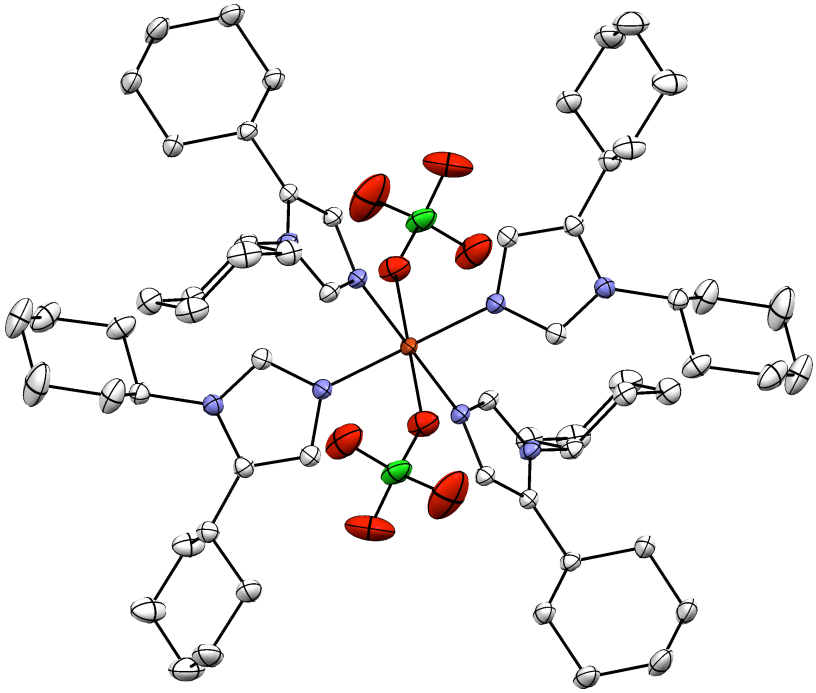

Figure S7. Displacement ellipsoid plot (50% probability) of the complex $[(DCHIm)_4Cu^{II}](ClO_4)_2 \cdot Et_2O$ at 110(2) K. The diethyl ether solvate molecule and H atoms are omitted for clarity.

Table S2. Distances (Å) and angles (°) for complex $(DCHIm)_4Cu^{II}(ClO_4)_2 \cdot Et_2O$.

Distance (Å)	
Cu-N1	1.996(13)
Cu-N2	1.996(1)
Cu-N3	2.0037(12)
Cu-N4	2.004(3)
Cu-O1	2.6046(13)
Cu-O2	2.605(1)
Angles (°)	
N1-Cu-N2	180.00(5)
N1-Cu-N3	91.12(5)
N1-Cu-N3*	88.88(5)
N1-Cu-O1	92.63(5)
N1-Cu-O1*	87.37(5)
N1*-Cu-N2*	180.00(5)

[(DCHIm)$_2$Cu^I](BArF): In the glovebox, 0.5 ml of a MeTHF solution containing 100 mg of [Cu^I(CH$_3$CN)$_4$](BArF) (0.11 mmols) were added dropwise to a 0.5 mL solution where 51 mg of DCHIm have been dissolved (0.22 mmols, MeTHF). The crude solution was stirred for 30 minutes, and 10 mL of pentane were added, leading to the formation of a white precipitate (Yield = 90%). Recrystallization of white powder led to formation of the desired [(DCHIm)$_2$Cu^I](BArF) (see below) in the form of colorless crystals, which were analyzed by X-Ray diffraction (**Figure S8**). Elemental analysis: ($C_{54}H_{48}N_4CuBF_{20}$) Calculated: C, 53.7%; H, 4.01%, N, 4.64%. Found: C, 53.9%; H, 4.02%; N, 4.45%. ESI-MS: 527.32 [(DCHIm)$_2$Cu^I]$^+$.

X-Ray characterization of [(DCHIm)$_2$Cu^I](BAr^F):

All reflection intensities were measured at 110(2) K using a SuperNova diffractometer (equipped with Atlas detector) with Cu *K*α radiation (λ = 1.54178 Å) under the program CrysAlisPro (Version 1.171.36.32 Agilent Technologies, 2013). The program CrysAlisPro (Version 1.171.36.32 Agilent Technologies, 2013) was used to refine the cell dimensions. Data reduction was done using the program CrysAlisPro (Version 1.171.36.32 Agilent Technologies, 2013). The structure was solved with the program SHELXS-2013 (Sheldrick, 2013) and was refined on F^2 with SHELXL-2013 (Sheldrick, 2013). Analytical numeric absorption corrections based on a multifaceted crystal model were applied using CrysAlisPro (Version 1.171.36.32 Agilent Technologies, 2013). The temperature of the data collection was controlled using the system Cryojet (manufactured by Oxford Instruments). The H atoms were placed at calculated positions using the instructions AFIX 13, AFIX 23 or AFIX 43 with isotropic displacement parameters having values 1.2 times *U*eq of the attached C atoms.

The structure is mostly ordered. One of the two imidazole rings N1→C3 is found to be disordered over two orientations (both orientations overlap, but the positions of N2 and C2 can interchange between the two orientations. The occupancy factor of the major component of the disorder refines to 0.713(17).

xs0269a: Fw = 1207.31, colorless lath, 0.43 × 0.15 × 0.09 mm^3, monoclinic, $P2_1/n$ (no. 14), a = 11.4059(2), b = 31.7761(5), c = 15.3471(3) Å, β = 111.604(2)°, V = 5171.58(17) Å^3, Z = 4, D_x = 1.551 g cm^{-3}, μ = 1.628 mm^{-1}, abs. corr. range: 0.645–0.898. 33635 Reflections were measured up to a resolution of (sin $\theta/\lambda)_{max}$ = 0.62 Å^{-1}. 10135 Reflections were unique (R_{int} = 0.0280), of which 8605 were observed [$I > 2\sigma(I)$]. 722 Parameters were refined. $R1/wR2$ [$I > 2\sigma(I)$]: 0.0354/0.0846. $R1/wR2$ [all refl.]: 0.0436/0.0892. S = 1.025. Residual electron density found between −0.49 and 0.33 e Å^{-3}.

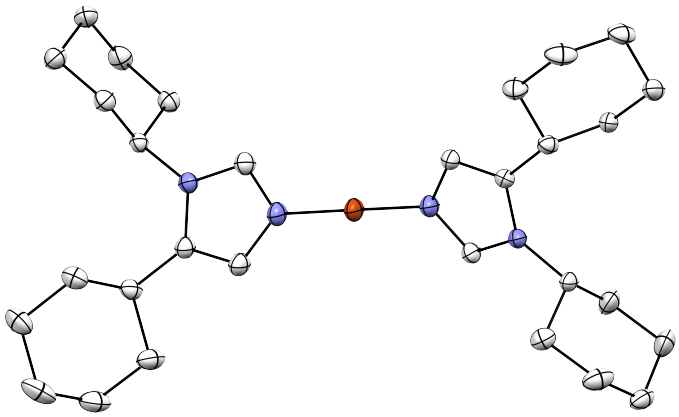

Figure S8. Displacement ellipsoid plot (50% probability) of complex [Cu^I(DCHIm)$_2$](BAr^F) at 110(2) K. The BAr^{F-} counter ion and H atoms are omitted for clarity. Cu-N = 1.8736(15)/1.8743(15) Å; N1-Cu-N3 angle = 177.99(7) º

5. DFT calculations: Density functional theory (DFT) calculations were performed using Gaussian09, version D.01. Geometry optimizations were done with the BP86 functional, employing a split basis set as follows: 6-311g* for Fe, Cu, and peroxo O atoms; 6-31g* for all metal-bound N atoms, and 6-31g for all remaining atoms. Tight SCF convergence and an ultrafine integration grid were used. All cyclohexyl substituents on DCHIm ligands were truncated as isopropyl groups in order to lower the computational cost, yet still capture some of the inherent steric effects.

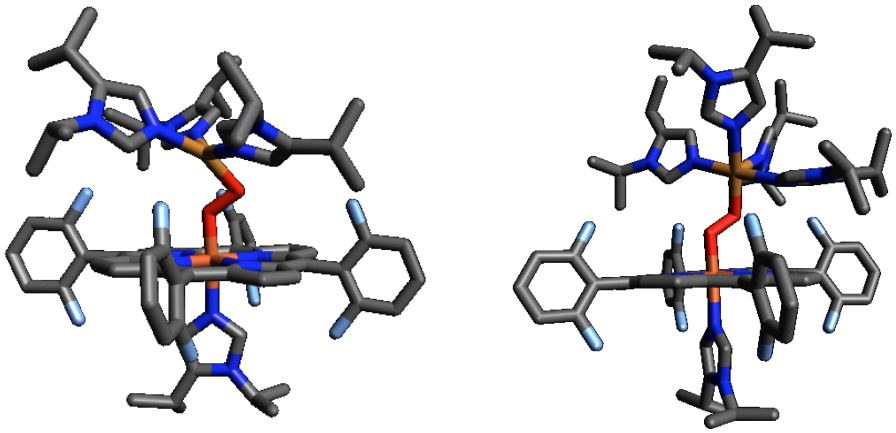

	LS-3DCHIm	**LS-4DCHIm**
δ Fe–O (Å)	1.807	1.842
δ O–O (Å)	1.401	1.366
δ Cu–O (Å)	1.914	1.947
δ Cu---Fe (Å)	4.102	4.473
∡ Fe–O–O (°)	121.5	118.6
∡ O–O–Cu (°)	92.4	111.7
Tau value	0.4 (0 = sqr. planar; 1 = tetrahedral)	0.09 (0 = sqr. pyr; 1 = trig. bipyr.)

Figure S9 & Table. Optimized structures of **LS-3DCHIm** (left) and **LS-4DCHIm** (right) and selected bond lengths and angles.

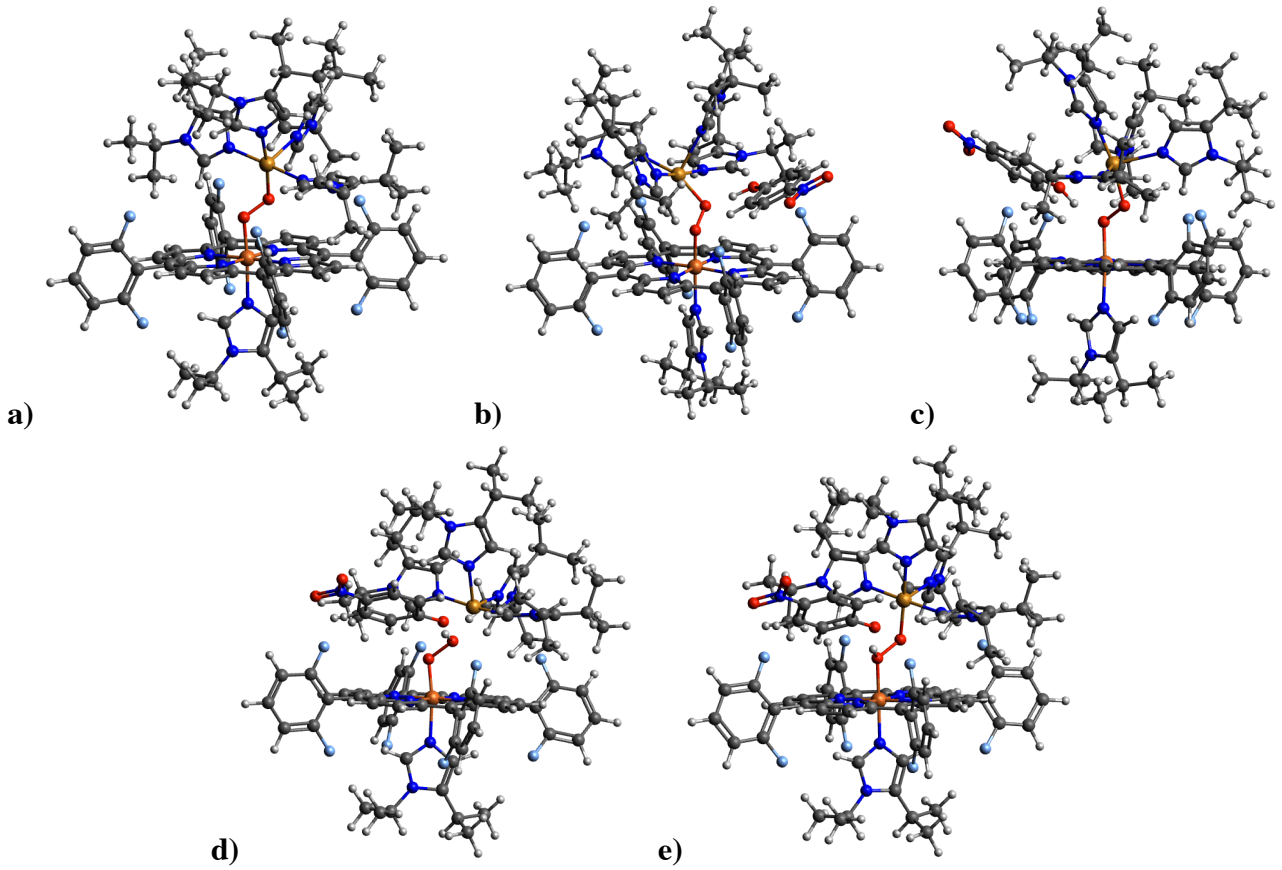

Figure S10. Structures for different [**(LS-4DCHIm)(ArOH)]** binding modes, corresponding to those given in **Table S3**.

Table S3. Relative free energies, bond lengths, Mayer Bond Orders (MBOs), and Mulliken Charges (on peroxo O atoms) for different possible phenolic binding modes for [**(LS-4DCHIm)(ArOH)]**.

	Structure	Rel. ΔG (kcal/mol)	*r*(Fe-O) (Å)	Fe-O MBO	*r*(O-O) (Å)	O-O MBO	O_{Fe} Mulliken Charge	O_{Cu} Mulliken Charge
(a)	**LS-4DCHIm**	--	1.842	0.685	1.366	0.929	-0.28	-0.36
(b)	**LS-4DCHIm + NO_2PhOH (H-bonded to O_{Cu})**	0	1.833	0.717	1.411	0.856	-0.31	-0.48
(c)	**LS-4DCHIm + NO_2PhOH (H-bonded to O_{Fe})**	+1.8	1.873	0.581	1.399	.874	-0.39	-0.37
(d)	**LS-4DCHIm + NO_2PhOH (with H^+ transferred to O_{Cu})**	+2.0	1.821	0.725	1.471	0.815	-0.34	-0.50
(e)	**LS-4DCHIm + NO_2PhOH (with H^+ transferred to O_{Fe})**	+7.4	1.927	0.435	1.438	0.835	-0.44	-0.39

6. EPR quantification of heme and Cu products of the reaction, LS-4DCHIm + 4-NO_2-phenol + Fc*:

Quantitation of Cu(II) and Fe(III)-containing products following the reaction of **LS-4DCHIm** with 4-NO_2-phenol and Fc* was carried out by spectral addition of the authentic spectra of the mononuclear species proposed in the text (**Figure 5**) (See page **S7-8** for the synthesis of the mononuclear species).

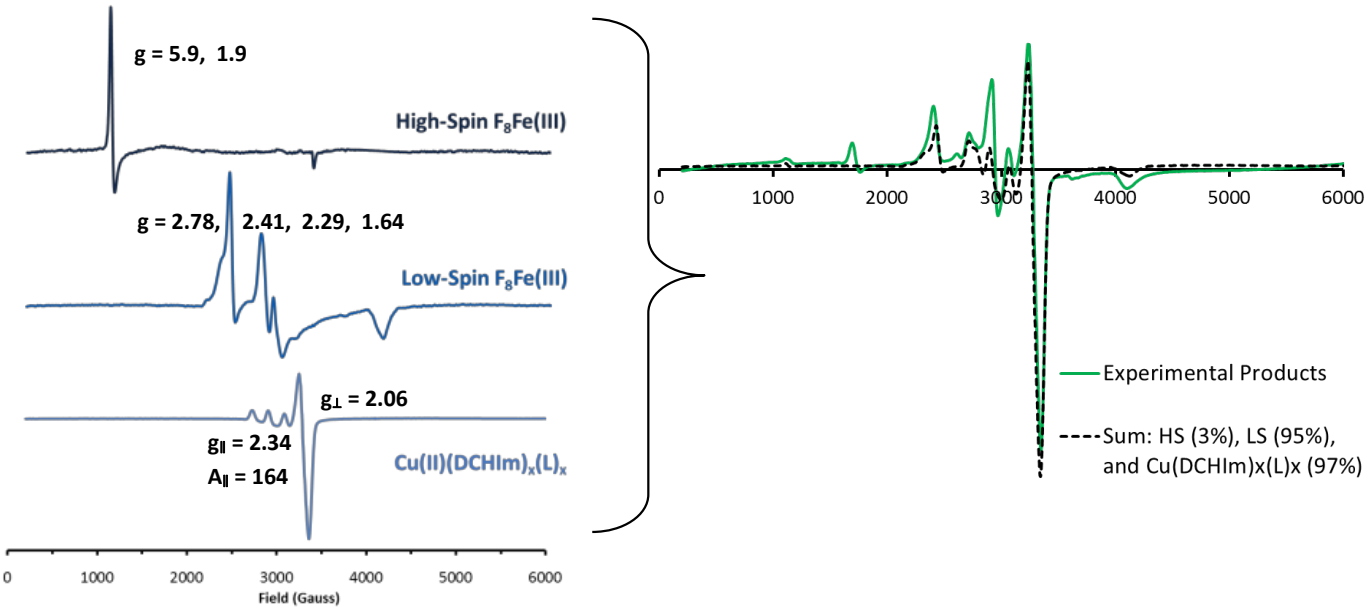

Figure S11: Quantification of the iron(III) and copper(II) products was carried out by comparing the reaction spectra with calibration curves obtained by generation of these species independently. This method allowed for confirmation of a mostly low-spin (~95%) heme product.

Authentic HS heme is ($F_8Fe^{III}\cdot SbF_6$), authentic LS-heme is ($F_8Fe^{III}(DCHIm)_2$) generated by addition of 2 equiv DCHIm to $F_8Fe^{III}\cdot SbF_6$, and authentic $Cu(II)(DCHIm)_x(L)_x$ spectrum shown on the left is that of $Cu(II)(DCHIm)_4(ClO_4)_2\cdot Et_2O$, see page **S7-8** for synthesis and X-ray crystallographic characterization. An identical EPR spectrum is generated when $Cu(II)(ClO_4)_2(H_2O)_6$ is exposed to even just 3 equiv DCHIm in MeTHF. Thus L (in **Figure 5** in the main text) is either DCHIm or MeTHF.

7. Resonance Raman Spectroscopy: The $^{16}O_2$, and $^{18}O_2$ spectra of the final product mixture, were compared with the authentic heme product, $F_8Fe^{III}(DCHIm)_2{\cdot}SbF_6$ for comparison (authentic $F_8Fe^{III}(DCHIm)_2{\cdot}SbF_6$ was generated by addition of 2 equiv DCHIm to $F_8Fe^{III}{\cdot}SbF_6$). No isotope sensitive bands are observed in the products, and both product spectra heme bands match nicely with the control, consistent with our formulation of the heme product as the bis-imidazole ferric heme species (see **Fig 5** in text). Samples were prepared at 1mM in MeTHF at -90°C, according to the following guidelines (for the reaction products): Generation of LS-4DCHIm was followed by addition of 10 eq Fc* (only very slightly soluble at these higher concentrations), mixing for 5 minutes with Ar bubbling and finally addition of 10 eq 4-NO_2-phenol, and mixing for 30 min with Ar bubbling at -90°C to ensure a complete reaction.

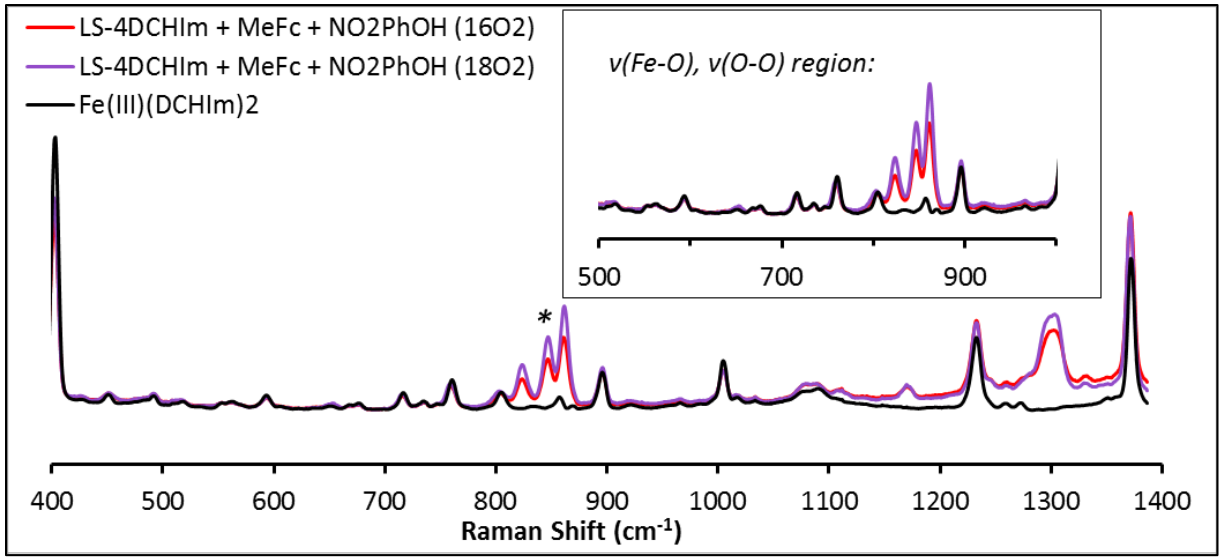

Figure S12: $^{16}O_2$ (red), and $^{18}O_2$ (purple) spectra of the final reaction products following reduction show no isotope sensitive vibrations, and match well with the control, Fe(III) bis-imidazole complex (black). These data were taken at 77 K with $\lambda_{excitation}$ = 413 nm.
*Note: From a spectrum of phenol(ate) in MeTHF, we attribute the sharp features between 800-900 cm^{-1}, as well as those at 1110, 1170, and 1300 cm^{-1}, to a phenolate or Cu(II)-phenolate species.

8. Kinetics: Reaction between (LS-4DCHIm) + 4-NO_2-phenol + Fc*. Kinetic experiments were carried out at different concentrations of the (**LS-4DCHIm**), (4-NO_2-phenol) or (Fc*). The k_{obs} were calculated by initial rates approximation (spectra taken every 1 sec), using the difference in the absorbance between 785 nm and 870 nm, which corresponded to the formation of Fc^{*+}. UV-Vis spectra of the reaction products indicated formation of 2 equivalents of Fc^{*+} along with formation of the low-spin iron(III) complex (DCHIm)F_8Fe^{III}(L) (λ_{max} = 542 nm) and a copper(II)-imidazolyl species (broad bands between 900-1100 nm) (see **Figure S6, S13**). The reaction rates obtained in the kinetic experiments are summarized in **Table S4**.

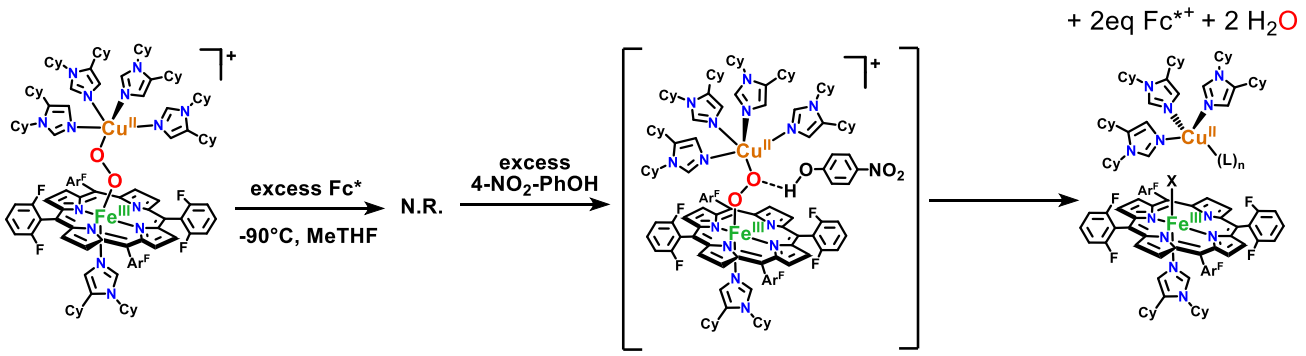

Figure S13. Reaction scheme for kinetic analysis of the reaction between (**LS-4DCHIm**) + 4-NO_2-phenol (H^+) and Fc* (e^-). Reductant was added first resulting in no reaction, and after addition of phenol, formation of the H-bond associated intermediate was observed before generation of the final products.

Table S4. Summary of kinetic experiments for the H^+/e^- reactivity of (**LS-4DCHIm**).

[(**LS-4DCHIm**)] (mM)	[4-NO_2-phenol] (mM)	[Fc*] (mM)	Rate (M^{-1} s^{-1})	k_{obs} (s^{-1})
0.06	2	4	$3.58 \cdot 10^{-7}$	0.0060
0.09	2	4	$4.88 \cdot 10^{-7}$	0.0054
0.135	2	4	$9.40 \cdot 10^{-7}$	0.0070
0.2	2	4	$1.42 \cdot 10^{-6}$	0.0071
0.135	0.5	4	$4.16 \cdot 10^{-7}$	0.0031
0.135	1	4	$7.00 \cdot 10^{-7}$	0.0052
0.135	2	4	$9.40 \cdot 10^{-7}$	0.0070
0.135	4	4	$1.30 \cdot 10^{-6}$	0.0097
0.135	2	1	$2.96 \cdot 10^{-7}$	0.0022
0.135	2	2	$3.76 \cdot 10^{-7}$	0.0028
0.135	2	4	$9.40 \cdot 10^{-7}$	0.0070
0.135	2	6	$1.34 \cdot 10^{-6}$	0.0099

[(LS-4DCHIm)] dependence. After generation of the low-spin complex (**LS-4DCHIm**) at different concentrations (0.09, 0.135 and 0.2 mM) in a typical UV-Vis experiment at -90 ºC, 30 μL of a solution containing Fc* [4.0 mM] were added, which didn't cause any spectral change. Addition of 4-NO_2-phenol [2.0 mM] caused a fast shift in the low-energy bands (750-1100 nm) (**Figure S14a**) along with the Q-band region from 537 to 540 nm due to the formation the hydrogen bonded complex, **[(LS-4DCHIm)(ArOH)].** Formation of the one-electron oxidation product Fc^{*+} was confirmed by the growth of a UV-Vis band at 780-800 nm and it was quantified (ε = 580 M^{-1} cm^{-1}, $Abs_{(785\text{-}870)}$) to confirm the 2-electron reduction. A shift on the Q-band from 540 to 542 nm was observed, confirming the formation of the $[(DCHIm)F_8Fe^{III}(L)](BAr^F)$ product (see **Figure S6**) along with the formation of a low-energy band between 800-1100 nm, assigned to the formation of a copper(II)-imidazolyl complex. The k_{obs} (normalized by the conc. of (**LS-4DCHIm**)) showed independence towards the concentration of the (**LS-4DCHIm**), indicating that only one molecule of heme-peroxo-complex is involved in the r.d.s., ruling out disproportion processes.

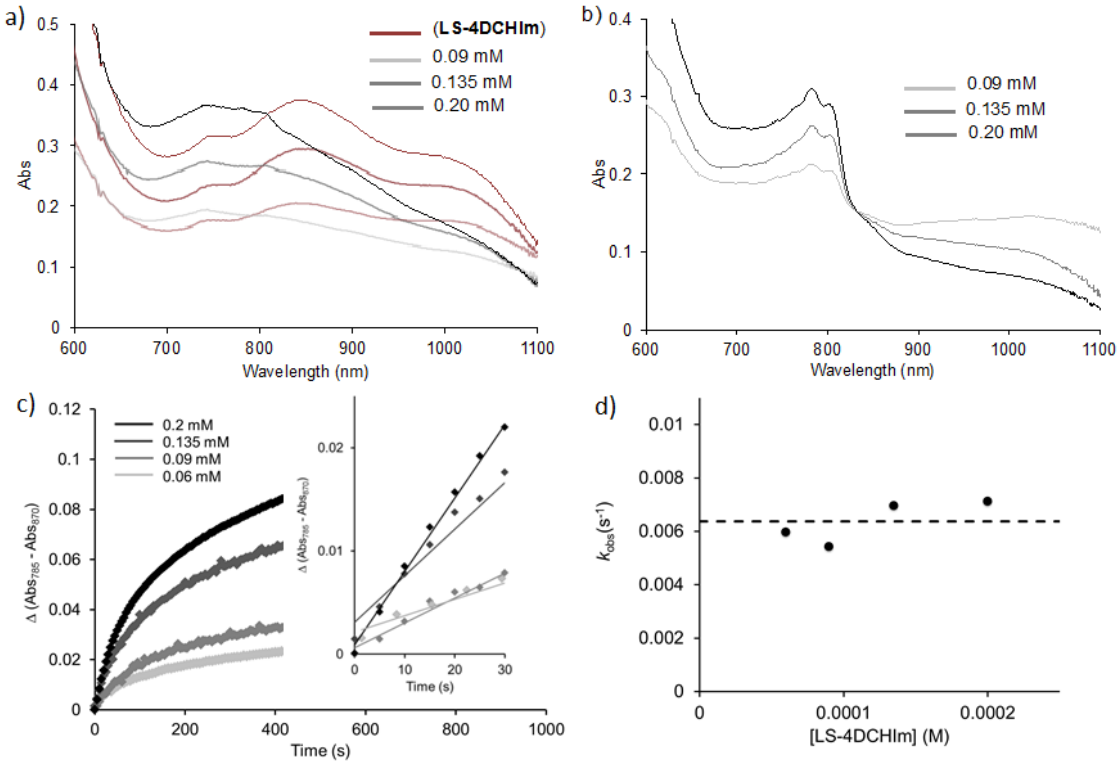

Figure S14. UV-Vis spectra and kinetic traces for the sequential reaction between (**LS-4DCHIm**) [0.09-0.2 mM], Fc* [4 mM] and 4-NO_2-phenol [2 mM]. (**a**) Initial spectra after addition of 4-NO_2-phenol (grey spectra) to (**LS-4DCHIm**) complex (brown spectrum). (**b**) Final spectra of the reaction observing the formation of 2 equiv. of Fc^{*+} and the copper(II) species (800-1100 nm). (**c**) Kinetic traces for the reduction between (**LS-4DCHIm**) [0.09 – 0.2 mM], Fc* [4 mM] and 4-NO_2-phenol [2 mM] (inset: initial rates observed). (**d**) k_{obs} vs. [**LS-4DCHIm**].

[4-NO_2-phenol] dependence. After generation of the low-spin complex (**LS-4DCHIm**) [0.135 mM] in a typical UV-Vis experiment at -90 ºC, 30 μL of a solution containing Fc* [0.4 mM] were added, which didn't cause any spectral change. Addition of different concentrations of 4-NO_2-phenol [0.5-4.0 mM] caused a fast shift in the low-energy bands (750-1100 nm) (**Figure S15a**) along with the Q-band region from 537 to 540 nm due to the formation the hydrogen bonded complex, **[(LS-4DCHIm)(ArOH)].** Formation of the one-electron oxidation product Fc^{*+} was confirmed by the growth of a UV-Vis band at 780-800 nm and it was quantified (ε = 580 M^{-1} cm^{-1}, $Abs_{(785-870)}$) to confirm the 2-electron reduction. A shift on the Q-band from 540 to 542 nm was observed, confirming the formation of the [(DCHIm)F_8Fe^{III}(L)](BAr^F) product (**See Figure S6**) along with the formation of a low-energy band between 800-1100nm, assigned to the formation of a copper(II)-imidazolyl complex. Curiously, at higher concentrations of phenol the low-energy bands were shifted to higher energies, suggesting that the final Cu(II)-imidazolyl species suffered a protonation or phenol/phenolate coordination. The k_{obs} (normalized by the conc. of (**LS-4DCHIm**)) showed a saturation behavior towards the concentration of the 4-NO_2-phenol, indicating only a pre-equilibrium or association process prior to the r.d.s.

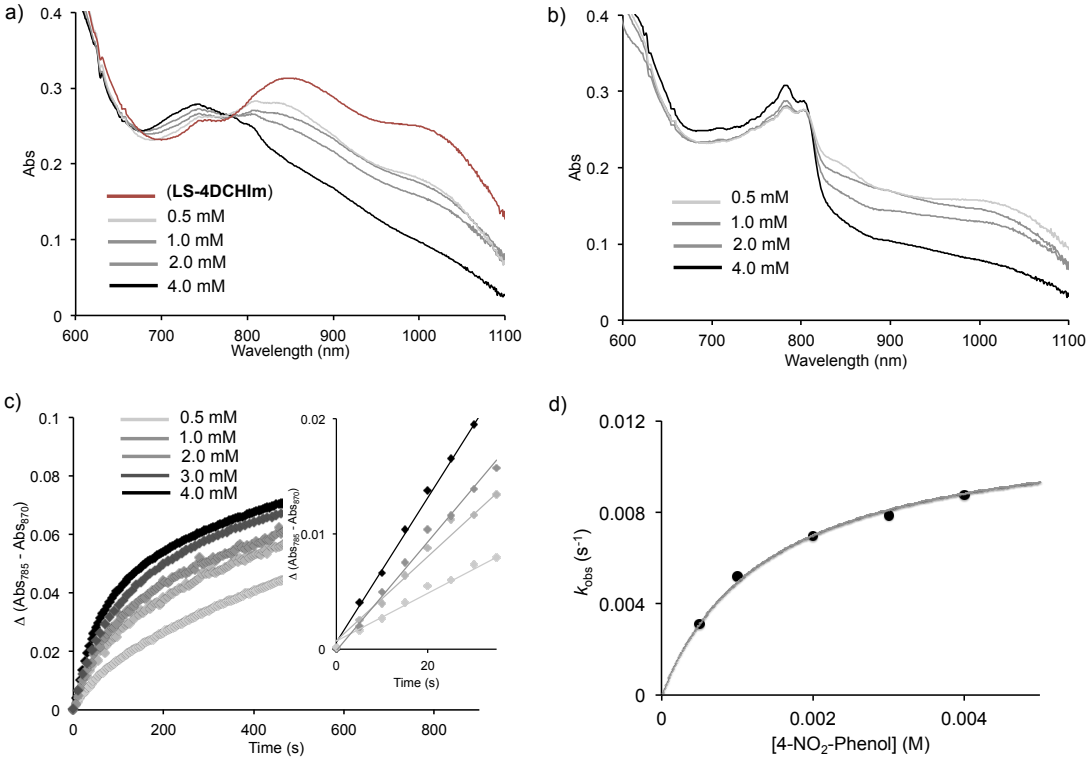

Figure S15. UV-Vis spectra and kinetic traces for the sequential reaction between (**LS-4DCHIm**) [0.135 mM], Fc* [4 mM] and 4-NO_2-phenol [0.5 - 4.0 mM]. (**a**) Initial spectra after addition of different quantities of 4-NO_2-phenol (grey spectra) to (**LS-4DCHIm**) (**brown spectrum**). (**b**) Final spectra of the reaction observing the formation of 2 equiv. of Fc^{*+} and the Cu^{II} species (800-1100 nm). (**c**) Kinetic traces for the reaction between (**LS-4DCHIm**) [0.135 mM], Fc* [4mM] and 4-NO_2-phenol [0.5-4.0 mM] (inset: initial rates observed). (**d**) k_{obs} vs. [4-NO_2-phenol].

[Fc*] dependence. After generation of the low-spin complex (**LS-4DCHIm**) [0.135 mM] in a typical UV-Vis experiment at -90 ºC, 30 μL of a solution containing different concentrations of Fc* [2.0-6.0 mM] were added, which didn't cause any spectral change. Addition of 4-NO_2-phenol caused a fast shift in the low-energy bands (750-1100 nm) (**Figure S16a**) along with the Q-band region from 537 to 540 nm due to the formation the hydrogen bonded complex, **[(LS-4DCHIm)(ArOH)].** Formation of the one-electron oxidation product Fc^{*+} was confirmed by the growth of a UV-Vis band at 780-800 nm and it was quantified (ε = 580 M^{-1} cm^{-1}, $Abs_{(785-870)}$) to confirm the 2-electron reduction. A shift on the Q-band from 540 to 542 nm was observed, confirming the formation of the $[(DCHIm)F_8Fe^{III}(L)](BAr^F)$ product (see **Figure S6**) along with the formation of a low-energy band between 800-1100 nm, assigned to the formation of a copper(II)-imidazolyl complex. The k_{obs} (normalized by the conc. of (**LS-4DCHIm**)) showed a linear dependence towards the concentration of the (Fc*), indicating that during the r.d.s., one molecule of the reductant is involved (single electron transfer r.d.s.).

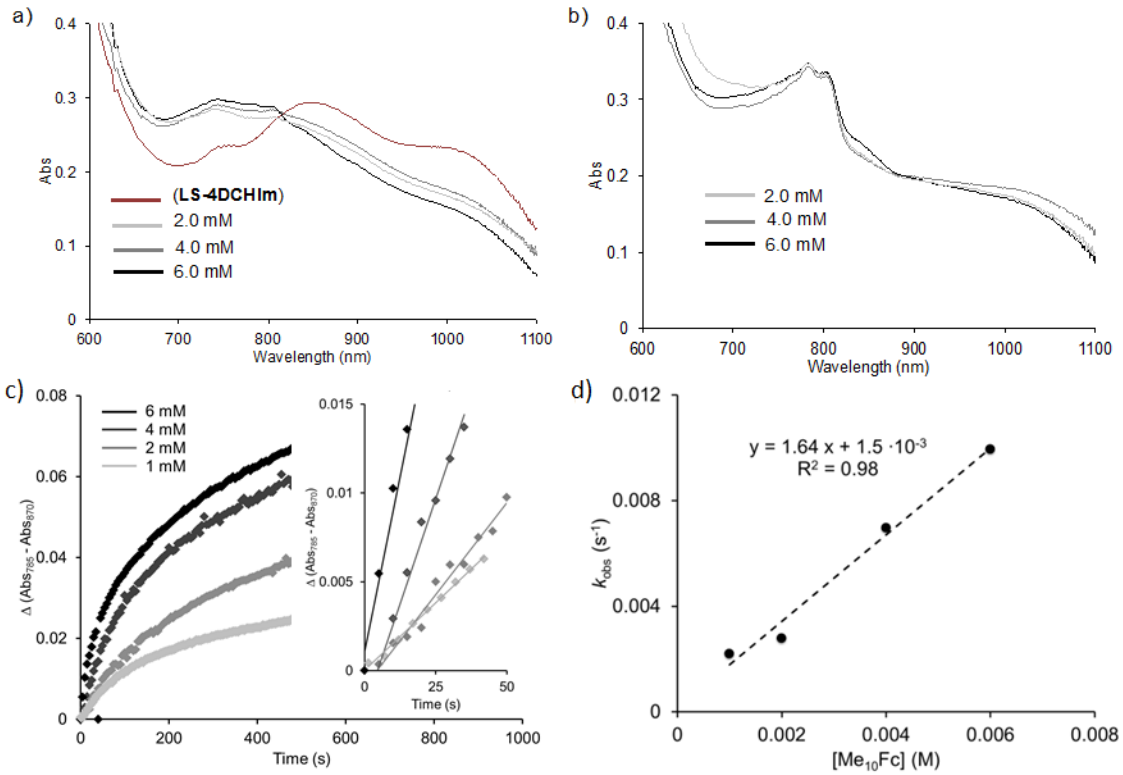

Figure S16. UV-Vis spectra and kinetic traces for the sequential reaction between (**LS-4DCHIm**) [0.135mM], Fc* [2-6 mM] and 4-NO_2-phenol [2.0mM]. (**a**) Initial spectra after addition of 4-NO_2-phenol (grey spectra) to (**LS-4DCHIm**) complex + Fc* (**brown spectrum**). (**b**) Final spectra of the reaction observing the formation of 2 equiv. of Fc^{*+} and the copper(II) species (800-1100nm). (**c**) Kinetic traces for the reduction between (**LS-4DCHIm**) [0.135 mM], Fc* [2.0 – 6.0 mM] and 4-NO_2-phenol [2.0 mM] at different concentrations of Fc* (inset: initial rates observed). (**d**) k_{obs} vs. [Fc*].

9. Synthesis and characterization of deuterated 4-NO_2-phenol, and KIE experiments: 100 mg 4-NO_2-PhONa (see **p. S19** for synthesis) was dissolved in a small amount of acetic acid-*d* (~3mL) and stirred for 30 minutes. The solvent was removed by vacuum, and the reaction crude was redissolved in ~5 mL freshly distilled MeTHF. The precipitated sodium acetate was filtered off with a fine frit and solvent was removed from the collected filtrate to afford the desired deuterated phenol product. ^{1}H-NMR of the product was taken in DMSO, and integration of relevant peaks revealed 85% deuteration at the hydroxy position. While this degree of isotopic labeling is not ideal for truly quantitative KIE measurements, a kinetic isotope effect is apparent and that observation alone gives support of our mechanistic hypothesis. Kinetics experiments and analysis were carried out as previously described (*vide supra*), with the results summarized in **Table S5**. k_{H+}/k_{D+} = 1.61 for the equilibrium process of weak acid association, and 1.84 for the rate determining PCET step (**Figure S17**).

Table S5. Summary of kinetic experiments for the D^+/e^- reactivity of (**LS-4DCHIm**).

[(**LS-4DCHIm**)] (mM)	[4-NO_2-phenol-**OD**] (mM)	[Fc*] (mM)	Rate (M^{-1} s^{-1})	k_{obs} (s^{-1})
0.135	0.5	4	$3.07 \cdot 10^{-7}$	0.00203
0.135	1	4	$5.43 \cdot 10^{-7}$	0.00381
0.135	2	4	$8.26 \cdot 10^{-7}$	0.00594
0.135	4	4	$1.27 \cdot 10^{-6}$	0.00673
0.135	2	1	$5.21 \cdot 10^{-7}$	0.00320
0.135	2	2	$6.85 \cdot 10^{-7}$	0.00421
0.135	2	4	$9.44 \cdot 10^{-7}$	0.00579
0.135	2	6	$1.26 \cdot 10^{-6}$	0.00774

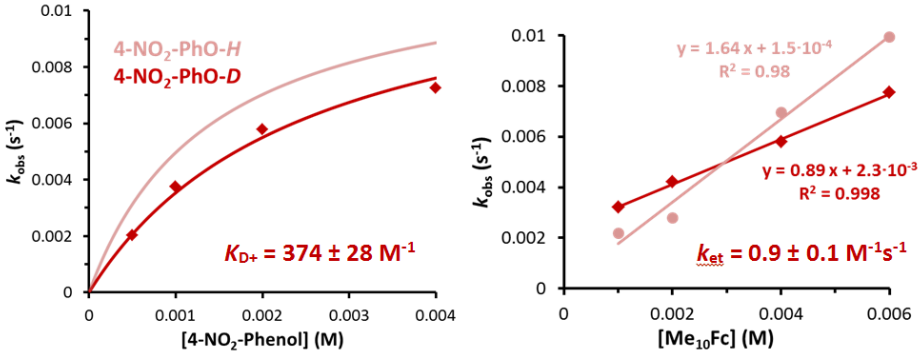

(a) $\text{KIE} = {}^{K_{H^+}}/_{K_{D^+}} = {}^{604}/_{374} = 1.61 \pm 0.06$

(b) $\text{KIE} = {}^{k_{et}(H^+)}/_{k_{et}(D^+)} = {}^{1.64}/_{0.89} = 1.84 \pm 0.09$

Figure S17. k_{obs} as a function of phenol concentration (0.5 – 4mM) (left) and as a function of Fc* concentration (1 – 6mM) (right) (PhOH = **pink trace**, PhOD = **dark red trace**). K_{D+} was calculated and the data fit according to the kinetic model shown in **Figure 6c** in the text. (a) Calculation of the deuterium Kinetic Isotope Effect for the equilibrium phenol association process and (b) for the rate determining electron transfer step.

10. Weak acid control experiments:

(a) *Synthesis and control reactions of relevant sodium phenolate:*
Approximately 100 mg of 4-NO_2-phenol was dissolved in 10 mL methanol. To that solution, a slight excess (1.1 equiv.) of NaOH was added and the mixture was stirred for 30 minutes. Solvent was removed completely under vacuum overnight, and the following day, recrystallized in diethylether, to afford a golden yellow solid which was characterized by ^{1}H-NMR in $(CD_3)_2SO$, (δ 5.86 (d, 2H); 7.69 (d, 2H)) and is only slightly soluble in MeTHF:

Table S6. UV-vis spectroscopic properties of the 4-NO_2-phenol the sodium phenolate.

Compound	***λ_{max} (nm)***	***ε (M^{-1} cm^{-1})***
4-NO_2-phenol	314	5,800
4-NO_2-PhO^- $^+$Na	393	14,800

Reactivity of sodium 4-NO_2-phenolate:

To probe the possible involvement of the weak acid conjugate base (phenolates are slightly basic and could be coordinating), excess (>10 equiv.) phenolate was added to the reaction mixture at each step. No spectral changes were observed by UV-vis except increases in intensity at the corresponding phenolate λ_{max} indicating that the conjugate bases do not affect the reactivity in any way and do not replace the monodentate copper DCHIm ligands.

(b) *Workup of organic reaction products:*

After a solution of **LS-4DCHIm** (0.1mM) + 10eq 4-NO_2-phenol + 10eq Fc* was allowed to react to completion in a Schlenk cuvette, solvent was immediately removed by rotary evaporation, and the products redissolved in pentane. The insoluble inorganic products were filtered off with a fine frit and the pentane was removed from the collected filtrate. A ^{1}H-NMR spectrum taken of the organic product in $(CD_3)_2SO$ showed only 4-NO_2-phenol (δ 6.92 ppm (d, 2H); 8.11 (d, 2H); 11.03 (s, 1H)) with no evidence of oxidized phenol or phenolate.

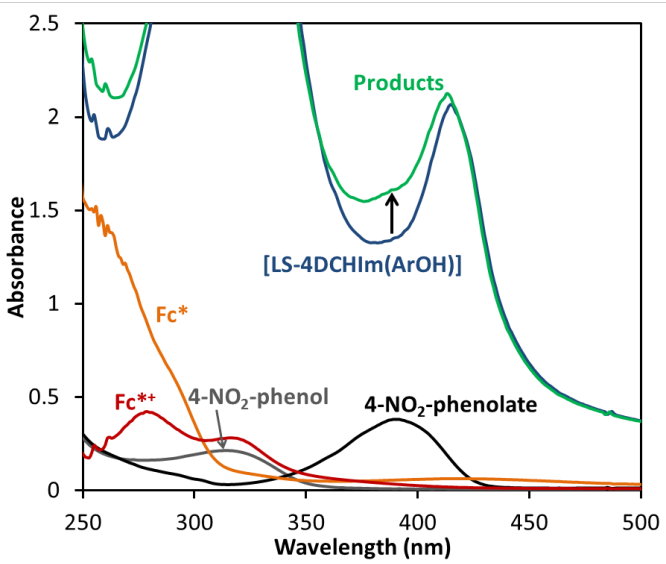

Figure S18. Shown here are the spectra of the adduct, **[LS-4DCHIm(ArOH)]** (**blue**, 0.02mM) and final products (**green**) where we observe a shoulder on the product Soret band due to absorbance of the 4-NO_2-phenolate present after protons are transferred. Separate spectra of the other reagents in solution show that none would contribute to this increase in absorbance at 393 nm. All independent reagent spectra are shown at 0.02 mM concentration, and using the epsilon value reported in **Table S6**, we quantified the phenolate to be approximately 1.4 equiv. Four protons are theoretically transferred in the peroxo to water transformation, however our rR data (see **Figure S12**) suggest that some phenolate may coordinate to the Cu(II) product.

11. References:

(1) Peterson, R. L.; Ginsbach, J. W.; Cowley, R. E.; Qayyum, M. F.; Himes, R. A.; Siegler, M. A.; Moore, C. D.; Hedman, B.; Hodgson, K. O.; Fukuzumi, S.; Solomon, E. I.; Karlin, K. D. *J. Am. Chem. Soc.* **2013**, *135*, 16454.

(2) Wang, J.; Schopfer, M. P.; Puiu, S. C.; Sarjeant, A. A. N.; Karlin, K. D. *Inorg. Chem.* **2010**, *49*, 1404.

(3) Favier, I.; Duñach, E. *Tetrahedron Lett.* **2004**, *45*, 3393.